Can New Physics Hide inside the Proton?

Stefano Carrazza,[1] Celine Degrande,[2] Shayan Iranipour,[3] Juan Rojo,[4,5] and Maria Ubiali[3,*]
[1]Tif Lab, Dipartimento di Fisica, Università di Milano and INFN, Sezione di Milano, Via Celoria 16, I-20133 Milano, Italy
[2]Centre for Cosmology, Particle Physics and Phenomenology (CP3), Université Catholique de Louvain, B-1348 Louvain-la-Neuve, Belgium
[3]DAMTP, University of Cambridge, Wilberforce Road, Cambridge, CB3 0WA, United Kingdom
[4]Department of Physics and Astronomy, VU University Amsterdam, De Boelelaan 1081, NL-1081, HV Amsterdam, Netherlands
[5]Nikhef, Science Park 105, NL-1098 XG Amsterdam, Netherlands

(Received 20 May 2019; revised manuscript received 20 August 2019; published 26 September 2019)

Modern global analyses of the structure of the proton include collider measurements which probe energies well above the electroweak scale. While these provide powerful constraints on the parton distribution functions (PDFs), they are also sensitive to beyond the standard model (BSM) dynamics if these affect the fitted distributions. Here we present a first simultaneous determination of the PDFs and BSM effects from deep-inelastic structure function data by means of the NNPDF framework. We consider representative four-fermion operators from the SM effective field theory (SMEFT), quantify to which extent their effects modify the fitted PDFs, and assess how the resulting bounds on the SMEFT degrees of freedom are modified. Our results demonstrate how BSM effects that might otherwise be reabsorbed into the PDFs can be systematically disentangled.

DOI: 10.1103/PhysRevLett.123.132001

Searches for physics beyond the standard model (BSM) at high-energy colliders can be divided into two main categories: direct searches, aiming to detect the production of new heavy particles, and indirect searches, whose goal is to identify subtle deviations in the interactions and properties of the SM particles. The latter would arise from virtual quantum effects involving BSM dynamics at energies well beyond the collider center-of-mass energy. Both strategies are actively pursued at the LHC by exploiting its unique energy reach [1] and its thriving program of precision measurements [2–4].

In this context, the SM effective field theory (SMEFT) [5–13] represents a powerful model-independent approach to identify, interpret, and correlate potential BSM effects from precision measurements under the assumption that the new physics scale, Λ, is well above the energies probed by the experimental data. Here, BSM effects can be parametrized at low energies in terms of dimension-six operators $\mathcal{O}_i$, constructed from SM fields satisfying its symmetries:

$$\mathcal{L}_{\mathrm{SMEFT}} = \mathcal{L}_{\mathrm{SM}} + \sum_{i=1}^{N} \frac{a_i}{\Lambda^2} \mathcal{O}_i, \tag{1}$$

where $\mathcal{L}_{\mathrm{SM}}$ is the SM Lagrangian, $\{a_i\}$ are the Wilson coefficients parametrizing the high-energy BSM dynamics, and N is the number of nonredundant operators. These Wilson coefficients can be constrained from measurements ranging from Higgs, gauge boson, and electroweak precision observables [14–17] to top quark production [18,19], flavor observables [20,21], and low-energy processes [22], among others. In the case of LHC data, high-energy processes such as Drell-Yan, diboson, and top-quark production at large invariant masses [23–29] play a key role since energy-growing effects often enhance the sensitivity to the SMEFT contributions.

Several of the high-energy LHC measurements that constrain the SMEFT parameter space are also used to provide stringent constraints on the proton's parton distribution functions (PDFs) [30,31]. Prominent examples include the large-x gluon from top-quark pair [32,33] and jet production [34,35], and the quark-flavor separation from high-mass Drell-Yan and W and Z boson production in association with jets [36–39]. This implies that BSM effects, if present in the high-energy tails of those distributions, could end up being "fitted away" into the PDFs. These concerns are particularly acute for the full exploitation of the run II and III datasets, as well as from the high-luminosity phase [40] where many PDF-sensitive observables will reach the few-TeV region [41].

In this work, we want to address two main questions. First, how can one assess whether BSM effects have been absorbed into the fitted PDFs? And second, how are the bounds on the SMEFT coefficients modified if the PDFs

used as input to determine them had been fitted using a consistent BSM theory? To answer them, we present here a first simultaneous determination of the proton's PDFs and the SMEFT Wilson coefficients $\{a_i\}$ by means of the NNPDF framework [42–45]. As a proof of concept, we consider the constraints from deep-inelastic scattering (DIS) structure functions on representative four-fermion operators. This way, we are able to quantify to which extent SMEFT effects (which parametrize general BSM dynamics) can be reabsorbed into the flexible neural-network based PDF parametrization [46]. This has required extending the NNPDF framework such that cross sections can be evaluated including BSM corrections at the fit level. We also assess how the bounds on the SMEFT coefficients are modified in this joint fit as compared to the traditional approach where PDFs are kept fixed. See Refs. [47,48] for related `xFitter` [49] studies restricted to H1 and ZEUS data and to one-parameter fits.

Here we study the impact of operators of the form

$$\mathcal{O}_{lq} = e^2(\bar{l}_R\gamma^\mu l_R)(\bar{q}_R\gamma_\mu q_R), \qquad q = u, d, s, c, \quad (2)$$

where l_R and q_R stand for right-handed charged leptons and quarks fields. We assume coupling universality in the lepton sector but not in the quark one, in order to evade the strong constraints from LEP precision data [50]. These operators lead to energy-growing effects and their contributions are weighted by the corresponding PDFs, two properties that provide powerful handles for discriminating them.

The calculation of the SMEFT corrections from the $\mathcal{O}_{lq}$ operators in Eq. (2) to DIS structure functions can be performed in analogy with the corresponding SM computation. For instance, F_2 will now contain terms linear and quadratic in a_u, the coefficient of $\mathcal{O}_{lu}$ in Eq. (1):

$$\Delta F_2^{\text{smeft}} \supset \left(\frac{a_u}{3}\frac{Q^2}{\Lambda^2}(1 + 4K_Z s_W^4) + \frac{a_u^2}{4}\frac{Q^4}{\Lambda^4}\right) \times (xu(x, Q^2) + x\bar{u}(x, Q^2)), \quad (3)$$

where $K_Z = Q^2/(4c_W^2 s_W^2(Q^2 + M_Z^2))$, $s_W = \sin\theta_W$, $c_W = \cos\theta_W$, and u ($\bar{u}$) represents the up (anti-)quark PDF. The terms linear in a_u arise from the interference with the SM amplitudes and are suppressed as Q^2/Λ^2. Similar expressions can be evaluated for the contributions from $\mathcal{O}_{ld}$, $\mathcal{O}_{ls}$, and $\mathcal{O}_{lc}$, and for the parity-violating structure function xF_3, while $\Delta F_L^{\text{smeft}} = 0$ at leading order. In this work we will keep only the leading $\mathcal{O}(\Lambda^{-2})$ terms in Eq. (3), though we have verified that results are stable upon the addition of the $\mathcal{O}(\Lambda^{-4})$ ones. These SMEFT-augmented structure functions have been implemented into `APFEL` [51,52]. The DGLAP equations for the scale evolution of the PDFs are unaffected, given that by construction the SMEFT assumes that there are no new light colored degrees of freedom (d.o.f.) that would modify the collinear singularities structure of QCD.

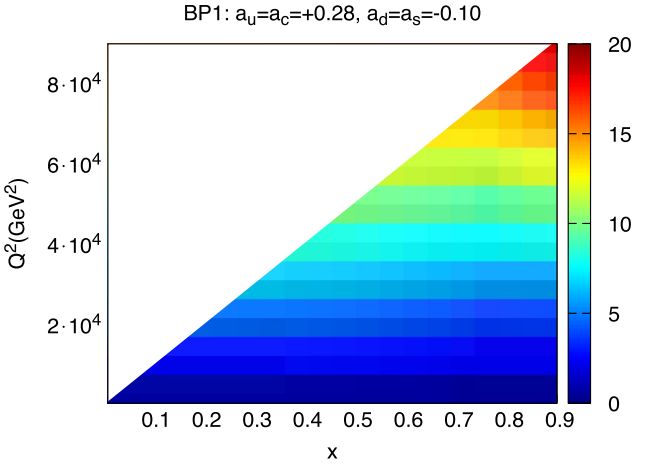

FIG. 1. The percentage SMEFT-induced shift, Eq. (4), for the e^-p neutral current DIS cross section at $\mathcal{O}(Q^2/\Lambda^2)$ for a representative choice of $\{a_q\}$ as a function of x and Q^2.

Since SMEFT effects are suppressed as Q^2/Λ^2, only measurements involving large momentum transfers Q^2 will be sensitive to them. The only DIS experiment that has explored the region $Q \gtrsim M_W$ is HERA [53], whose legacy structure function data [54] reach up to $Q_{\max} \simeq 250$ GeV. In Fig. 1 we display the percentage shift in the e^-p neutral current (NC) DIS cross section,

$$\Delta_{\text{smeft}} \equiv (d^2\sigma^{\text{NC}}/dxdQ^2)/(d^2\sigma^{\text{NC}}_{\text{SM}}/dxdQ^2) - 1, \quad (4)$$

as a function of x and Q^2, for a specific choice of coefficients given by $a_u = a_c = 0.28$ and $a_d = a_s = -0.10$. As in the rest of the Letter, we assume here that $\Lambda = 1$ TeV. The corrections depend only mildly on Bjorken-x and increase rapidly with Q, reaching up to $\simeq$20% for the upper HERA kinematic limit. In the case of positron-proton scattering the x dependence would be stronger, but the Q^2 dependence would cancel out between the F_2 and F_3 terms; see the Supplemental Material [55].

Given that for a sizable region of the SMEFT parameter space the shifts Eq. (4) are comparable or bigger than the experimental uncertainties of the precise HERA structure functions, the latter can be exploited to impose bounds on the allowed ranges of the coefficients $\{a_q\}$. First of all, we evaluate the values of $\chi^2_{\text{tot}}(\{a_q\})$ for the DIS measurements used in NNPDF3.1 [56], corresponding to $n_{\text{dat}} = 3092$ data points from BCDMS, SLAC, NMC, CHORUS, NuTeV, and HERA. In this calculation, we use NNPDF3.1 NNLO DIS-only as input with consistent theory settings such as FONLL-C [57] and fitted charm [58]. This is repeated for a range of SMEFT benchmark points (BPs) (listed in the Supplemental Material [55]) and for the $N_{\text{rep}} = 100$ Monte Carlo replicas.

TABLE I. The 90% C.L. intervals (for $\Lambda = 1$ TeV) for the coefficients extracted with fixed PDFs, comparing individual and marginalized bounds with and without PDF uncertainties.

		Marginalized	
	Individual	no PDF unc	w PDF unc
a_u	$[-0.1, +0.4]$	$[-2.3, +1.4]$	$[-3.6, +2.7]$
a_d	$[-1.6, +0.4]$	$[-13, +3.9]$	$[-19, +11]$
a_s	$[-2.8, +4.2]$	$[-18, +29]$	$[-36, +47]$
a_c	$[-2.6, +1.2]$	$[-13, +7.0]$	$[-21, +15]$

The resulting $\chi^2_{\rm tot}(\{a_q\})$ values are then fitted to a quadratic form,

$$\chi^2_{\rm min} + \sum_{q,q'=u,d,s,c} H_{qq'}(a_q - a_q^{(\rm min)})(a_{q'} - a_{q'}^{(\rm min)}), \quad (5)$$

where $H_{qq'}$ are the elements of the Hessian matrix in the quark flavor space. Note that Eq. (5) is exact if the $\mathcal{O}(\Lambda^{-4})$ corrections are neglected, else it is valid only close to a local minimum. We have performed the fits of the SMEFT coefficients both varying a single operator at a time (individual fits) as well as varying the four of them simultaneously and then marginalizing over each one.

In Table I we indicate the 90% confidence level (C.L.) intervals for the four coefficients obtained with fixed input PDFs. We compare the individual bounds with the marginalized ones from the four-dimensional fits, without and with PDF uncertainties. In the former case, theory calculations are obtained using the central replica. In the latter case, we compute the bounds for the $N_{\rm rep} = 100$ replicas and take the envelope of the 90% narrower ones.

The most stringent bounds are obtained for a_u, followed by a_d, and then a_c and a_s. This is consistent with the fact that the SMEFT corrections proportional to a_q are weighted by the corresponding PDFs in Eq. (3), and that in the HERA region $u(x) \gtrsim d(x) \gg s(x), c(x)$. The marginalized bounds are looser than the individual ones by up to an order of magnitude, highlighting the relevance of exploring simultaneously the widest possible region of the parameter space. PDF uncertainties turn out to be moderate. For the individual fits, the bounds are stable upon the inclusion of $\mathcal{O}(Q^4/\Lambda^4)$ terms.

The main limitation of the bounds reported in Table I is that they might be affected by double counting, since the same HERA data were already included in the NNPDF3.1 fit used here to evaluate the DIS structure functions with SMEFT effects. The very same problem arises for the interpretation of collider measurements that are used to constrain both the PDFs and the SMEFT parameter space, such as jet, Drell-Yan, and top quark pair production. To bypass this limitation, the way forward is provided by the simultaneous extraction of the PDFs and the SMEFT d.o.f. $\{a_q\}$, in the same way as in joint extractions of PDFs and the strong coupling constant [59].

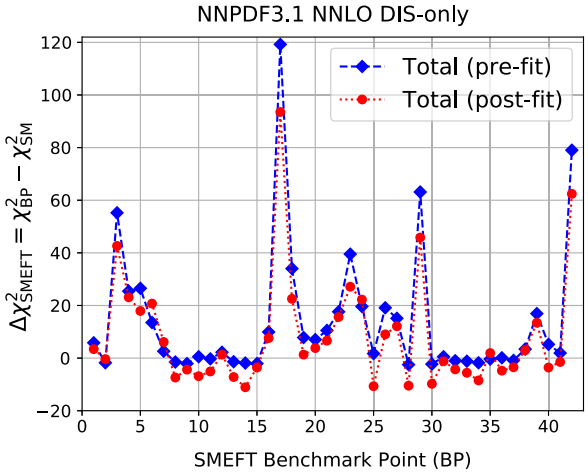

FIG. 2. The difference in $\chi^2_{\rm tot}$ with respect to the SM in the fits with different BPs, compared to the fixed-PDF results.

We have thus carried out variants of the NNPDF3.1 NNLO DIS-only fit now using as theory input the structure functions with SMEFT corrections. These fits have been performed for the same BPs as in the fixed-PDF analysis, and are based on 300 replicas to tame statistical fluctuations. Defining $\Delta\chi^2_{\rm smeft} = \chi^2_{\rm tot} - \chi^{2(\rm SM)}_{\rm tot}$, we find that the BP with the largest improvement (deterioration) with respect to the SM has $\Delta\chi^2_{\rm smeft} \simeq -10$ ($\simeq$90), see Fig. 2. In all cases, $\chi^2_{\rm tot}$ decreases as compared to the pre-fit (fixed-PDF) result, indicating that SMEFT effects are being partially reabsorbed into the PDFs.

From Fig. 2 one expects that in the fits with SMEFT corrections the resulting PDFs will be distorted as compared to their SM-based counterparts. Here the flexible NNPDF parametrization is suitable to robustly assess to what extent such effects can be reabsorbed into the PDFs. First, we find that the quark valence distributions are rather similar to those of the SM case, see the Supplemental Material [55]. The reason is that quark PDFs are dominantly fixed by the moderate Q^2 fixed-target DIS data, and thus unaffected by the high-Q^2 HERA structure functions.

More significant differences are observed for the gluon PDF. Within a DIS-only fit, the gluon is mostly constrained from the scaling violations between the low- and high-Q^2 data, which are strongly modified in the presence of energy-growing SMEFT effects. In Fig. 3 we show the gluon in the fits based on the $(a_u, a_d, a_s, a_c) = (-0.3, -1.8, -5, 5)$ and (0,1.2,10,0) BPs, normalized to the SM and where PDF uncertainties are only displayed for the latter. These are two of the BPs leading to the largest deviations from the SM at the χ^2 level, with $\Delta\chi^2_{\rm smeft} \simeq 65$ and 41, respectively, while also being consistent with the bounds from the HERA data in Table I. We find that the SMEFT-induced distortions can be comparable with the PDF uncertainties and thus should be taken into account.

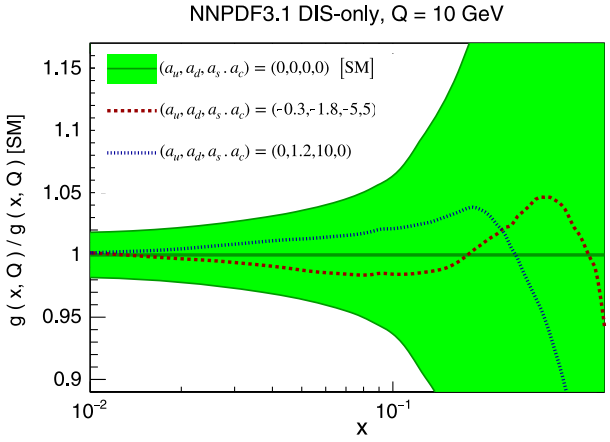

FIG. 3. The gluon PDF in the fits with two representative SMEFT BPs (for $\Lambda = 1$ TeV), normalized to the SM result.

These distortions would be even more pronounced in a global fit, where the gluon can be extracted with higher precision.

The different energy scaling of the SMEFT effects as compared to the QCD ones (polynomial in the former, logarithmic in the latter) can be exploited to disentangle BSM dynamics from QCD ones within the PDF fit. In Fig. 4 we display $\chi^2_{\rm hera}/n_{\rm dat}$ as a function of the cut $Q_{\rm max}$ that fixes the maximum value that enters the χ^2 evaluation. Results are shown both in the SM and in the SMEFT for $a_u = a_d = -1.3$ and $a_s = a_c = 0$, and in the latter case both for the prefit (fixed-PDF) and postfit cases. While for $Q_{\rm max} \gtrsim 50$ GeV the value of $\chi^2_{\rm hera}/n_{\rm dat}$ is flat for the SM case, there is a rapid degradation in the fit quality for the SMEFT case. This result further highlights that BSM effects cannot be completely fitted away. Such distinctive trend in the high-energy behavior of the theory would represent a smoking gun for BSM effects, similar to how

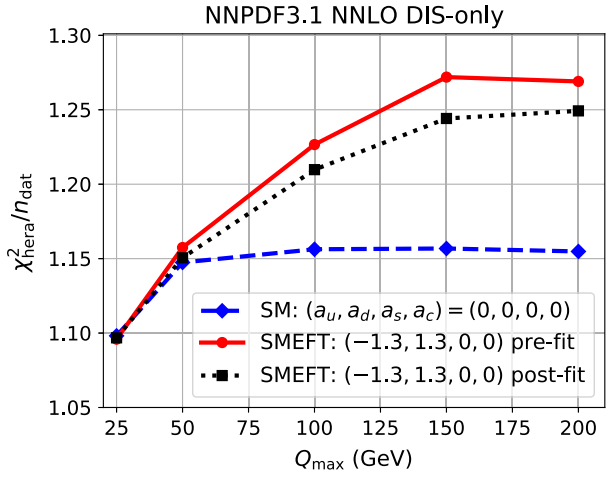

FIG. 4. The dependence of $\chi^2_{\rm hera}/n_{\rm dat}$ on $Q_{\rm max}$ in the case of the SM and for one representative SMEFT BP, for which we indicate both the prefit and the postfit values.

TABLE II. Same as Table I for the simultaneous determination of the PDFs and the SMEFT coefficients.

	Individual	Marginalised
a_u	$[0.0, +0.5]$	$[-0.4, +2.4]$
a_d	$[-1.1, +0.8]$	$[-4.4, +4.5]$
a_s	$[-4.5, +3.6]$	$[-61, +39]$
a_c	$[-2.4, +0.7]$	$[-29, +2.7]$

BFKL dynamics were recently identified from small-x HERA data [60].

In Table II we indicate the individual and marginalized 90% C.L. intervals for the SMEFT coefficients from this joint extraction together with the PDFs, see Table I for the fixed-PDF ones. We find that the bounds are rather similar in both cases, consistent with the evidence from Figs. 2–4 that SMEFT corrections are only partially reabsorbed in the PDFs. As expected, the individual limits are somewhat broader at the postfit level. The marginalized bounds are affected by a sizable statistical uncertainty associated with the finite number of replicas. The latter is estimated by Gaussianly fluctuating the $\chi^2_{\rm tot}$ values of each BP around their central values by their bootstrap uncertainty, and keeping only those fluctuations leaving a positive-definite Hessian. The distribution of fit minima, eigenvalues, and eigenvectors are used to estimate these statistical errors, finding in particular that they are larger than the central value associated to the smallest eigenvalue and that a flat direction, mainly in the $(a_s - a_c)$ plane, could not be excluded.

Other studies have quantified the constraints on four-fermion operators such as those of Eq. (2), and a compilation of the information from precision LEP data and low-energy measurements was presented in Ref. [22]. In Fig. 5 we compare the 90% C.L. bounds in the (a_u, a_d) plane from our work (both prefit and postfit level) with

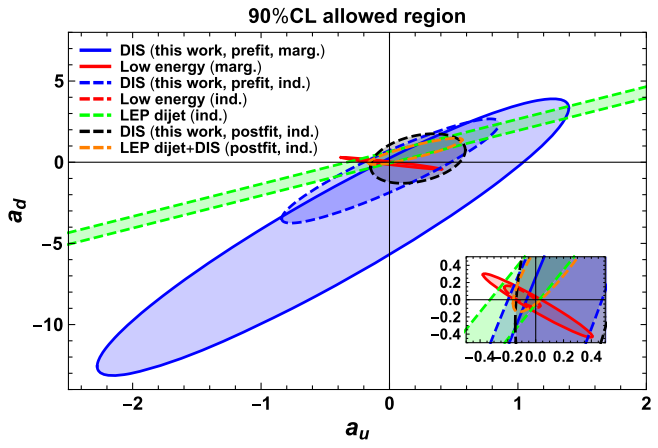

FIG. 5. The 90% C.L. marginalized and individual bounds in the (a_u, a_d) plane from this work compared to those from Ref. [22] (dijet and parity) and to the individual bound from dijet data.

those from both LEP dijet data and parity measurements. We also show the individual bounds from the former since, contrary to the parity data, these are independent on the modeling of the nucleon structure. We find that our precise bound for a_u is comparable to previous studies, while those for a_d, a_s, and a_c are less competitive. This encouraging result emphasizes the potential of high-energy collider data for the simultaneous extraction of both PDFs and SMEFT d.o.f.

To summarize, in this work we have systematically analyzed the interplay between PDF and SMEFT fits, using the HERA structure functions that provide the backbone of all modern PDF extractions as a case study. Our results represent the successful proof of concept of a program aiming to exhaustively disentangle potential BSM effects in high-energy measurements that might otherwise be reabsorbed into the PDFs. The next steps in this program will be to extend our study to a global dataset, including LHC data, and to a wider operator basis.

We are grateful to A. Falkowski, M. Gonzalez-Alonso, and K. Mimouni for discussions concerning Ref. [22]. We thank F. Maltoni, E. Mereghetti, T. You, B. Allanach, and the SUSY working group for insightful discussions. S. C. is supported by the European Research Council under the European Union's Horizon 2020 research and innovation Programme (Grant Agreement No. 740006). C. D. is supported by the Fund for Scientific Research F.N.R.S. through the F.6001.19 convention. J. R. is supported by the European Research Council Starting Grant No. "PDF4BSM" and by the Netherlands Organization for Scientific Research (NWO). M. U. and S. I. are partially supported by the STFC Grant No. ST/L000385/1 and the Royal Society Grant No. RGF/EA/180148. M. U. is funded by the Royal Society Grant DH150088.

*m.ubiali@damtp.cam.ac.uk

[1] S. Rappoccio, Rev. Phys. **4**, 100027 (2019).
[2] S. Dawson, C. Englert, and T. Plehn, Phys. Rep. **816**, 1 (2019).
[3] M. Cristinziani and M. Mulders, J. Phys. G **44**, 063001 (2017).
[4] J. Erler and M. Schott, Prog. Part. Nucl. Phys. **106**, 68 (2019).
[5] S. Weinberg, Physica (Amsterdam) **96A**, 327 (1979).
[6] W. Buchmuller and D. Wyler, Nucl. Phys. **B268**, 621 (1986).
[7] C. Arzt, M. B. Einhorn, and J. Wudka, Nucl. Phys. **B433**, 41 (1995).
[8] B. Grzadkowski, Z. Hioki, K. Ohkuma, and J. Wudka, Nucl. Phys. **B689**, 108 (2004).
[9] J. A. Aguilar-Saavedra, Nucl. Phys. **B812**, 181 (2009).
[10] D. Nomura, J. High Energy Phys. 02 (2010) 061.
[11] J. A. Aguilar-Saavedra, Nucl. Phys. **B843**, 638 (2011); **B851**, 443 (2011).
[12] B. Grzadkowski, M. Iskrzynski, M. Misiak, and J. Rosiek, J. High Energy Phys. 10 (2010) 085.
[13] I. Brivio and M. Trott, Phys. Rep. **793**, 1 (2019).
[14] J. Ellis, C. W. Murphy, V. Sanz, and T. You, J. High Energy Phys. 06 (2018) 146.
[15] A. Bierktter, T. Corbett, and T. Plehn, SciPost Phys. **6**, 064 (2019).
[16] E. S. Almeida, A. Alves, N. Rosa-Agostinho, O. J. P. Éboli, and M. C. Gonzalez-Garcia, Phys. Rev. D **99**, 033001 (2019).
[17] J. de Blas, M. Ciuchini, E. Franco, S. Mishima, M. Pierini, L. Reina, and L. Silvestrini, J. High Energy Phys. 12 (2016) 135.
[18] A. Buckley, C. Englert, J. Ferrando, D. J. Miller, L. Moore, M. Russell, and C. D. White, Phys. Rev. D **92**, 091501(R) (2015).
[19] N. P. Hartland, F. Maltoni, E. R. Nocera, J. Rojo, E. Slade, E. Vryonidou, and C. Zhang, J. High Energy Phys. 04 (2019) 100.
[20] J. Aebischer, J. Kumar, P. Stangl, and D. M. Straub, Eur. Phys. J. C **79**, 509 (2019).
[21] D. M. Straub, arXiv:1810.08132.
[22] A. Falkowski, M. Gonzalez-Alonso, and K. Mimouni, J. High Energy Phys. 08 (2017) 123.
[23] M. Farina, G. Panico, D. Pappadopulo, J. T. Ruderman, R. Torre, and A. Wulzer, Phys. Lett. B **772**, 210 (2017).
[24] A. Greljo and D. Marzocca, Eur. Phys. J. C **77**, 548 (2017).
[25] S. Alioli, M. Farina, D. Pappadopulo, and J. T. Ruderman, Phys. Rev. Lett. **120**, 101801 (2018).
[26] S. Alioli, W. Dekens, M. Girard, and E. Mereghetti, J. High Energy Phys. 08 (2018) 205.
[27] F. Maltoni, L. Mantani, and K. Mimasu, arXiv:1904.05637.
[28] S. Alte, M. König, and W. Shepherd, J. High Energy Phys. 01 (2018) 094.
[29] M. Farina, C. Mondino, D. Pappadopulo, and J. T. Ruderman, J. High Energy Phys. 01 (2019) 231.
[30] J. Butterworth *et al.*, J. Phys. G **43**, 023001 (2016).
[31] J. Gao, L. Harland-Lang, and J. Rojo, Phys. Rep. **742**, 1 (2018).
[32] M. Guzzi, K. Lipka, and S.-O. Moch, J. High Energy Phys. 01 (2015) 082.
[33] M. Czakon, N. P. Hartland, A. Mitov, E. R. Nocera, and J. Rojo, J. High Energy Phys. 04 (2017) 044.
[34] L. A. Harland-Lang, A. D. Martin, and R. S. Thorne, Eur. Phys. J. C **78**, 248 (2018).
[35] J. Rojo, Int. J. Mod. Phys. A **30**, 1546005 (2015).
[36] R. Boughezal, A. Guffanti, F. Petriello, and M. Ubiali, J. High Energy Phys. 07 (2017) 130.
[37] S. A. Malik and G. Watt, J. High Energy Phys. 02 (2014) 025.
[38] F. Giuli and (xFitter Developers' Team), Eur. Phys. J. C **77**, 400 (2017).
[39] Technical Report No. ATL-PHYS-PUB-2019-016, CERN, Geneva, 2019.
[40] P. Azzi *et al.* (HL-LHC, HE-LHC Working Group), arXiv: 1902.04070.
[41] R. Abdul Khalek, S. Bailey, J. Gao, L. Harland-Lang, and J. Rojo, Eur. Phys. J. C **78**, 962 (2018).
[42] R. D. Ball *et al.* (NNPDF Collaboration), J. High Energy Phys. 04 (2015) 040.

[43] R. D. Ball, V. Bertone, S. Carrazza, C. S. Deans, L. Del Debbio *et al.*. (NNPDF Collaboration), Nucl. Phys. **B867**, 244 (2013).
[44] R. D. Ball, L. Del Debbio, S. Forte, A. Guffanti, J. I. Latorre, A. Piccione, J. Rojo, and M. Ubiali (NNPDF Collaboration), Nucl. Phys. **B809**, 1 (2009).
[45] R. D. Ball, L. Del Debbio, S. Forte, A. Guffanti, J. I. Latorre, J. Rojo, and M. Ubiali (NNPDF Collaboration), Nucl. Phys. **B838**, 136 (2010).
[46] J. Rojo, arXiv:1809.04392.
[47] F. D. Aaron *et al.* (H1 Collaboration), Phys. Lett. B **705**, 52 (2011).
[48] H. Abramowicz *et al.* (ZEUS Collaboration), Phys. Rev. D **99**, 092006 (2019).
[49] S. Alekhin *et al.*, Eur. Phys. J. C **75**, 304 (2015).
[50] Z. Han and W. Skiba, Phys. Rev. D **71**, 075009 (2005).
[51] V. Bertone, S. Carrazza, and J. Rojo, Comput. Phys. Commun. **185**, 1647 (2014).
[52] V. Bertone, S. Carrazza, and N. P. Hartland, Comput. Phys. Commun. **212**, 205 (2017).
[53] M. Klein and R. Yoshida, Prog. Part. Nucl. Phys. **61**, 343 (2008).
[54] H. Abramowicz *et al.* (ZEUS and H1 Collaborations), Eur. Phys. J. C **75**, 580 (2015).
[55] See Supplemental Material at http://link.aps.org/supplemental/10.1103/PhysRevLett.123.132001 for additional information about the impact of SMEFT corrections to the DIS structure functions and about the fits based on theory calculations that include SMEFT corrections. We describe how we map the parameter space associated to the SMEFT four-fermion operators, and in particular present our choice of benchmark points. We quantify systematically the impact on the PDFs of the SMEFT corrections for each of the benchmark points and study in further detail their mutual correlation.
[56] R. D. Ball *et al.* (NNPDF Collaboration), Eur. Phys. J. C **77**, 663 (2017).
[57] S. Forte, E. Laenen, P. Nason, and J. Rojo, Nucl. Phys. **B834**, 116 (2010).
[58] R. D. Ball, V. Bertone, M. Bonvini, S. Carrazza, S. Forte, A. Guffanti, N. P. Hartland, J. Rojo, and L. Rottoli (NNPDF Collaboration), Eur. Phys. J. C **76**, 647 (2016).
[59] R. D. Ball, S. Carrazza, L. Del Debbio, S. Forte, Z. Kassabov, J. Rojo, E. Slade, and M. Ubiali (NNPDF Collaboration), Eur. Phys. J. C **78**, 408 (2018).
[60] R. D. Ball, V. Bertone, M. Bonvini, S. Marzani, J. Rojo, and L. Rottoli, Eur. Phys. J. C **78**, 321 (2018).